



## A coupled Volume Penalization-Thermal Lattice Boltzmann method for thermal flows

Xiongwei Cui <sup>a,\*</sup>, Xiongliang Yao <sup>a</sup>, Zhikai Wang <sup>a</sup>, Minghao Liu <sup>b</sup>

<sup>a</sup>College of Shipbuilding Engineering, Harbin Engineering University, Harbin 150001, China

<sup>b</sup>School for Engineering of Matter, Transport and Energy, Arizona State University, Tempe, AZ 85281, USA



### ARTICLE INFO

#### Article history:

Received 8 January 2018

Received in revised form 10 May 2018

Accepted 11 June 2018

Available online 14 July 2018

#### Keywords:

Heat transfer

Volume Penalization method

Thermal Lattice Boltzmann method

Immersed boundary method

Dirichlet boundary condition

Thermal flows

Fluid-solid interaction

### ABSTRACT

In this article, a coupled Volume Penalization-Thermal Lattice Boltzmann method is proposed to solve the thermal flow problem. The temperature Dirichlet boundary condition of the temperature field is ensured by introducing an external thermal penalization heat source term into the energy equation. Coupled with the Lattice Boltzmann-Volume Penalization method, which is used to simulated athermal flow past obstacles, the thermal flow problem can be solved. Besides, performing the Volume Penalization-Thermal Lattice Boltzmann method on a certain point, only the variables of this point are needed, which means the present method can be conducted parallelly. To verify the present method, the heat transfer between two concentric circular cylinders experiment is carried out firstly, in which the accuracy of the present method is also studied. Then natural convection between two concentric circular cylinders and between a cold square outer and a hot cylinder inner is performed to verify the present method further. To validate the ability of the method to solve the forced convection and mixed convection, the flows past a heated circular cylinder and the mixed convection of a heated rotating cylinder in a square enclosure are conducted. Good agreements between the present results and those in the previous literatures are achieved.

© 2018 Elsevier Ltd. All rights reserved.

## 1. Introduction

Lattice Boltzmann method, as an alternative to the traditional Navier-Stokes (N-S) equation solver, has been adopted to solve the problem relating to the interaction between fluid flows and obstacles widely [1]. The simplicity in coding, parallel and explicit calculation procedure are its three main advantages which contribute to its popularity. In the procedure of the solving the interaction between the fluid flows and the obstacles, especially when the boundary of the obstacles are complex, treating the obstacle boundaries is an extremely important point. Just like in the traditional N-S equation solvers, two main techniques: body-fitted grid method and the immersed boundary method are adopted to solve the interaction between the fluid flows and the obstacles in the Lattice Boltzmann method.

For the body-fitted grid method, generating a body-fitted grid is the first and important step, during which the structured and unstructured grids are frequently used. But this step is of great expense, especially when the some complex boundaries are involved. Even with simple boundaries, it is not easy to create a

high quality body-fitted grid. When the boundary of the obstacle moves or changes, the body-fitted grid should be regenerated every step and the variables on the last grid should be also interpolated to the new grid, which is prohibitive. Besides, the order of accuracy on the structured and unstructured grids is lower than that on the uniform Cartesian grids [2].

Compared with the body-fitted grid method, the immersed boundary method, proposed by Peskin [3], can be easily implemented. In the immersed boundary method, an external forcing term is introduced to the momentum equations to reflect the boundary effect of obstacles on the fluid flows, which is the extremely bright spot of immersed boundary method. For the modified momentum equations, there is no inner boundary, which means the modified momentum equations can be solved on a fixed uniform Cartesian grid. As a result, the generation and re-generation of the body-fitted grid are unneeded, even when the boundary of the obstacle moves or changes. The dynamics of the obstacles are represented by a Lagrangian grid. The information and variables on these two grids are related to each other by a discrete delta function interpolation. Interpolating the velocity on the boundary based on the velocity field of the Cartesian grid and spreading the force density to the Cartesian grid points near the boundary by using the delta function are two main steps in the immersed

\* Corresponding author.

E-mail address: [cuixiongwei@yahoo.com](mailto:cuixiongwei@yahoo.com) (X. Cui).

boundary method. After the immersed boundary method was firstly incorporated into the Lattice Boltzmann method by Feng and Michaelides [4], many types of the coupled immersed boundary method and Lattice Boltzmann method have been developed for the incompressible viscous fluid flows past obstacles such as: the direct-forcing IBM-LBM [5], velocity correct-based IBM-LBM [6], momentum exchange IBM-LBM [7] and so on. But here another interesting immersed boundary method is focused: the Volume Penalization (VP) method.

The Volume Penalization method, proposed by Arquis and Caltagirone [8], was incorporated into LBM by Benamour [9]. In the VP, the obstacles are considered as a porous medium with extremely small permeability. The boundary of the obstacle is modeled on the fixed grid by a mask function. Actually, the Lagrangian grid in the VP is part of the fixed Cartesian grid which is marked by the mask function. So each point of the Lagrangian grid coincides with a certain point of the fixed Cartesian grid. Compared with the direct forcing IBM and the velocity correction IBM, there is no need to interpolate the velocity at the boundaries and to spread the force density to the Cartesian grid points near the boundaries by the delta function. So performing the VP procedure on a certain Lagrangian grid point just needs the variables on a Cartesian grid point with which the Lagrangian grid point coincides, which means the VP procedure can be conducted parallelly. Taking the parallelizability of the LBM into consideration, the whole VP-LBM can be conducted parallelly. Besides, the solution of the penalized N-S equations tends towards the exact solution of the N-S equations imposing no-slip boundary conditions with the penalization parameter approaching zero [10–12]. Under the help of the forcing term proposed by Guo [13], the VP is incorporated into LBM successfully to simulate flows past obstacles [14].

In this article, the volume penalization method coupled with Lattice Boltzmann is applied to solve the heat transfer problem. The heat transfer problem is a very interesting issue which has attracted many researchers and has been used in many areas, such as the latest reported research micropolar fluids [15], fluid flow in porous enclosure [16,17] and thermal flows under the control of electric field [18–20]. Coupled with the Thermal Lattice Boltzmann method (TLBM), the immersed boundary methods mentioned above have been also used to solve the heat transfer and convection problem [21–23]. Besides, M. Sheikholeslami and his co-workers have adopted the Thermal Lattice Boltzmann to study the natural convection heat transfer problems under the magnetic field [24], which has opened a new area where the Thermal Lattice Boltzmann can be used. An external thermal penalization heat source term is introduced into the energy equation to enforce the temperature field at the boundaries satisfied the temperature Dirichlet boundary condition. The modified energy equation is solved by another population of Lattice Boltzmann model: Thermal Lattice Boltzmann method. Coupled with modified N-S equation solved by the Lattice Boltzmann method, the proposed method Volume Penalization-Thermal Lattice Boltzmann (VP-TLBM) is used to solve the thermal flow problem. To verify the proposed VP-TLBM and study the accuracy of the proposed method, the heat transfer between two concentric circular cylinders is conducted firstly. Then the natural convection between two concentrically placed horizontal circular cylinder and between a cold square outer and a hot circular cylinder inner is chosen as the experiment to verify the proposed method further.

The rest of this article is arranged as follows. In Section 2, the Lattice Boltzmann-Volume Penalization method firstly introduced briefly. Then the proposed VP-TLBM is introduced in details. The whole computational procedure is given in this section as well. In Section 3, the numerical experiments and the comparison of the results are given. Some concluding remarks and recommendations for the future work are presented in Section 4.

## 2. Mathematical and numerical formulation

In this section, the Lattice Boltzmann-Volume Penalization is introduced briefly. Then the proposed Volume Penalization-Thermal Lattice Boltzmann method is introduced in details. Finally, the whole computing procedure is given.

### 2.1. The Lattice Boltzmann-Volume Penalization method

Let us take the fluid-solid interaction (FSI) between incompressible viscous fluid and rigid boundary into consideration. The dynamics of the fluid can be governed by the following incompressible Navier-Stokes equation:

$$\frac{\partial \mathbf{u}}{\partial t} + \mathbf{u} \cdot \nabla \mathbf{u} + \frac{1}{\rho} \nabla p = \mu \nabla^2 \mathbf{u} + \mathbf{f} \quad (1)$$

$$\nabla \cdot \mathbf{u} = 0, \quad (2)$$

where  $\mathbf{u}$  is the velocity of the fluid,  $\mu$  is the dynamic viscosity,  $\rho$  is the density,  $p$  is the pressure and  $\mathbf{f}$  is the body force. The no-slip boundary conditions on the rigid boundary domain  $\Omega_o$  in the fluids can be described as:

$$\mathbf{u}|_{\partial\Omega_o} = \mathbf{U}_o, \quad (3)$$

where  $\partial\Omega_o$  is the boundary of the obstacles and  $\mathbf{U}_o$  is the velocity of the obstacles. The computational domain is shown in Fig. 1.  $\Omega_F$  is the fluid domain. The union of these two domains  $\Omega = \Omega_F \cup \Omega_o$  is the entire domain.

The Dirichlet problem Eqs. (1)–(3) can be solved by the Volume Penalization method [10,11]. In the Volume Penalization method, the solid obstacles are modeled as porous media. By adding a penalization term on the velocity, the momentum Eq. (1) is modified as:

$$\frac{\partial \mathbf{u}}{\partial t} + \mathbf{u} \cdot \nabla \mathbf{u} = -\frac{1}{\rho} \nabla p + \mu \nabla^2 \mathbf{u} + \mathbf{f} - \frac{\chi(\mathbf{x}, t)\rho}{\eta} (\mathbf{u} - \mathbf{U}_o), \quad (4)$$

where

$$\chi(\mathbf{x}, t) = \begin{cases} 1 & \mathbf{x} \in \Omega_o \\ 0 & \text{other} \end{cases} \quad (5)$$

is the mask function used to describe the obstacles' geometry and  $\eta \ll 1$  is the penalization parameter. It can be seen that there is no Dirichlet boundary condition in Eq. (4). The solution of the

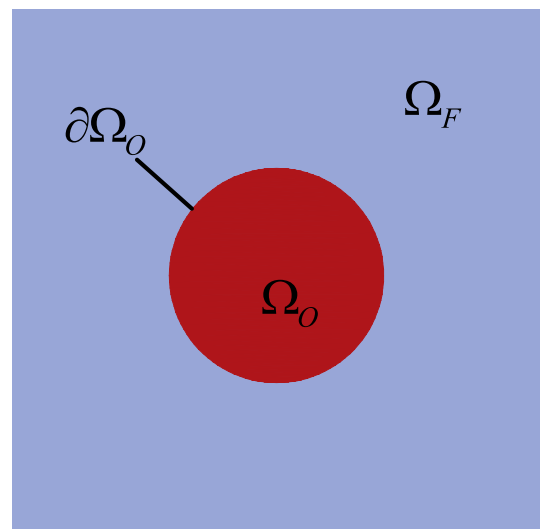


Fig. 1. The computational domain of boundary and fluid.

penalized N-S Eq. (4) tends towards the exact solution of N-S equation imposing no-slip boundary conditions with  $\eta \rightarrow 0$  [10–12]. The hydrodynamic forces acting on the obstacle can be obtained through:

$$\mathbf{F}_O = \lim_{\eta \rightarrow 0} \int_{\Omega} \frac{\chi\rho}{\eta} (\mathbf{u} - \mathbf{U}_0) d\Omega = \lim_{\eta \rightarrow 0} \int_{\Omega_0} \frac{\chi\rho}{\eta} (\mathbf{u} - \mathbf{U}_0) d\Omega. \quad (6)$$

The N-S equations can be recovered by the Lattice Boltzmann method equation by the multi-scale Chapman-Enskog analysis. The discrete Boltzmann equation with single-relaxation time (SRT) collision operator can be written as:

$$\frac{\partial f_\alpha}{\partial t} + \mathbf{e}_\alpha \cdot \nabla f_\alpha = -\frac{f_\alpha - f_\alpha^{eq}}{\lambda} + F_\alpha, \quad (7)$$

in which  $f_\alpha$  is the particle distribution function;  $t$  is the time;  $\mathbf{e}_\alpha$  is the particle velocity in the  $\alpha$ th direction;  $f_\alpha^{eq}$  is the equilibrium distribution function and  $\lambda$  is the relaxation parameter, which is related to the kinematic viscosity  $\nu$  through  $\nu = c_s^2(\lambda - 0.5)\Delta t$ , where  $c_s^2$  is the speed of sound;  $F_\alpha$  is the external forcing term. Eq. (7) can be split into two sub-steps [25]: collision

$$\hat{f}_\alpha = f_\alpha - \frac{f_\alpha - f_\alpha^{eq}}{\lambda} \quad (8)$$

and streaming

$$f_\alpha(\mathbf{x}, t + \Delta t) = \hat{f}_\alpha(\mathbf{x} - \Delta \mathbf{x}_\alpha, t). \quad (9)$$

For the nine-velocity lattice model in two dimension (D2Q9), the discrete velocity vectors are defined as:

$$\mathbf{e}_\alpha = \begin{cases} (0, 0), & \alpha = 0 \\ (\cos\theta_\alpha, \sin\theta_\alpha), & \theta_\alpha = (\alpha - 1)\pi/2, \alpha = 1 - 4 \\ \sqrt{2}(\cos\theta_\alpha, \sin\theta_\alpha), & \theta_\alpha = (2\alpha - 9)\pi/4, \alpha = 5 - 8 \end{cases}, \quad (10)$$

and the equilibrium distribution function can be expressed as:

$$f_\alpha^{eq} = \rho w_\alpha \left[ 1 + \frac{\mathbf{e}_\alpha \cdot \mathbf{u}}{c_s^2} + \frac{(\mathbf{e}_\alpha \cdot \mathbf{u})^2 - c_s^2 |\mathbf{u}|^2}{2c_s^4} \right], \quad (11)$$

in which  $c_s = 1/\sqrt{3}$  is the sonic speed and the weight factors are  $w_0 = 4/9$ ,  $w_{1-4} = 1/9$  and  $w_{5-8} = 1/36$ . The macroscopic density,  $\rho$ , and velocity,  $\mathbf{u}$  are defined as follows:

$$\rho = \sum_\alpha f_\alpha \quad (12)$$

$$\rho \mathbf{u} = \sum_\alpha \mathbf{e}_\alpha f_\alpha. \quad (13)$$

In this article, the external forcing term proposed by Guo et al. [26] is adopted:

$$F_\alpha = \left( 1 - \frac{1}{2\lambda} \right) w_\alpha \left( \frac{\mathbf{e}_\alpha - \mathbf{u}}{c_s^2} + \frac{\mathbf{e}_\alpha \cdot \mathbf{u}}{c_s^4} \cdot \mathbf{e}_\alpha \right) \cdot \mathbf{F}_{external}, \quad (14)$$

$$\rho \mathbf{u} = \sum_\alpha \mathbf{e}_\alpha f_\alpha + \frac{1}{2} \mathbf{F}_{external} \cdot \Delta t, \quad (15)$$

where  $\mathbf{F}_{external} = \mathbf{f} - \mathbf{F}_O$ .

From Eq. (15), the fluid velocity consists of two parts [6]. The density distribution function contributes the first part, which is represented by the intermediate velocity  $\mathbf{u}^*$ . And the second is contributed from the external forcing term  $\mathbf{F}_{external}$  which can be taken as velocity correction  $\delta\mathbf{u}$ . The intermediate velocity  $\mathbf{u}^*$  can be expressed as:

$$\rho \mathbf{u}^* = \sum_\alpha \mathbf{e}_\alpha f_\alpha \quad (16)$$

and the velocity correction  $\delta\mathbf{u}$  as

$$\rho \delta\mathbf{u} = \frac{1}{2} \mathbf{F}_{vp} \Delta t. \quad (17)$$

Eq. (15) can be rewritten as:

$$\mathbf{u} = \mathbf{u}^* + \delta\mathbf{u}. \quad (18)$$

Substituting Eq. (18) into Eq. (6), the forcing term contributed from the obstacles can be expressed as:

$$\mathbf{F}_O = \frac{(\mathbf{u}^* + \frac{\mathbf{f}_{At}}{2\rho} - \mathbf{U}_0)}{2\eta + \chi\Delta t}, \quad (19)$$

and the velocity correction can be obtained as:

$$\delta\mathbf{u} = \frac{\Delta t(2\eta\mathbf{f} + 2\rho\chi\mathbf{U}_0 - 2\rho\chi\mathbf{u}^*)}{2\rho(2\eta + \chi\Delta t)}. \quad (20)$$

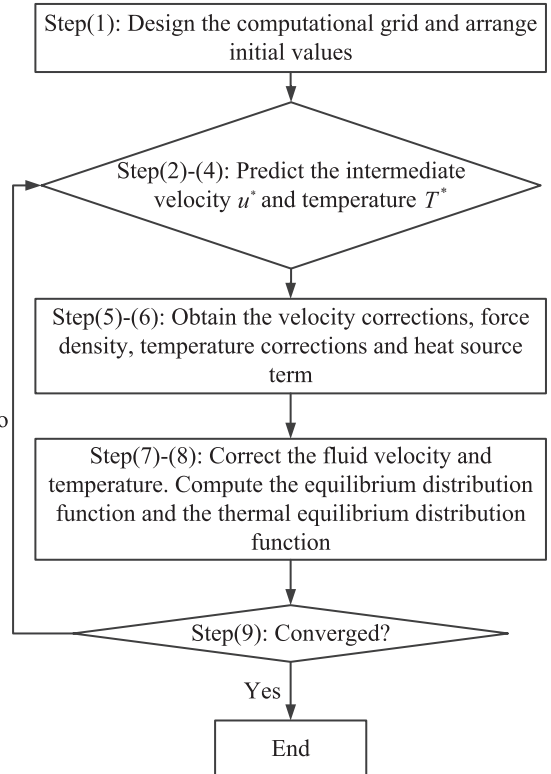


**Fig. 2.** The flowchart of the computational sequence of the Volume Penetration-Thermal Lattice Boltzmann method for thermal flows.

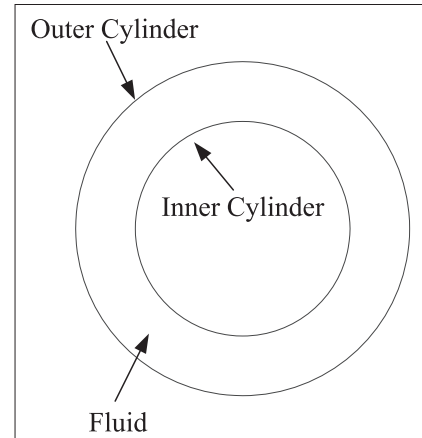
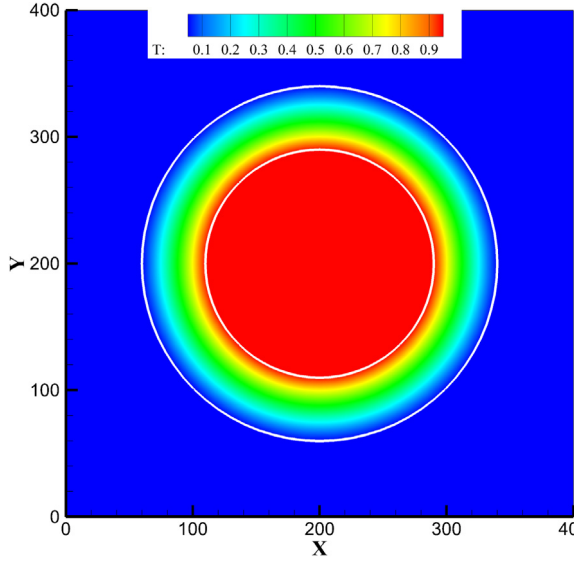
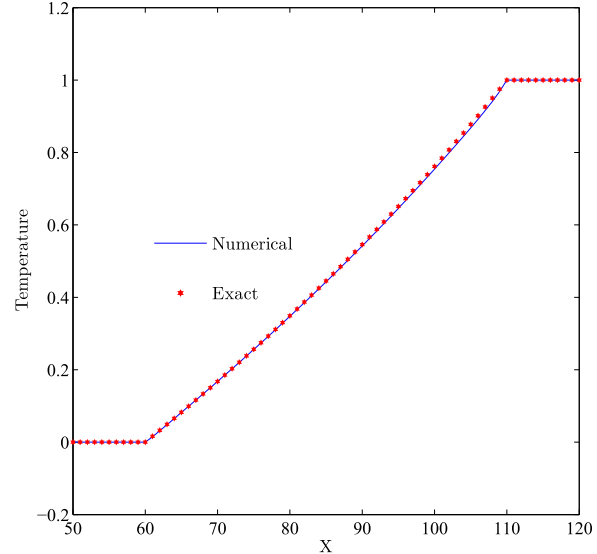


**Fig. 3.** The computational domain of the heat transfer between two concentric cylinders.



(a) Temperature contour



(b) Temperature profile along the horizontal plane through the center of the cylinders

**Fig. 4.** Temperature contour and profile between two concentric cylinders using  $400 \times 400$  grid sized.

## 2.2. The proposed Volume Penalization-Thermal Lattice Boltzmann method

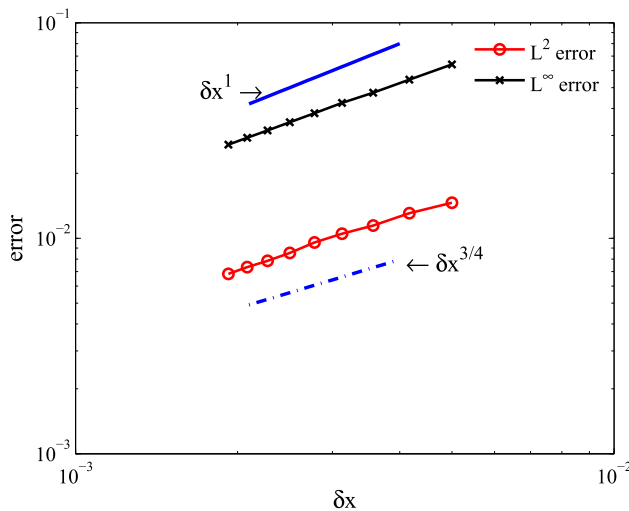
For the thermal fluid, the fluid temperature is governed by the following energy equation:

$$\frac{\partial T}{\partial t} + \mathbf{u} \cdot \nabla T = \kappa \nabla^2 T, \quad (21)$$

in which  $T$  is the temperature,  $\kappa$  is the thermal diffusivity. Just like in the Volume Penalization method for the athermal flows, we add an external thermal penalization heat source term  $Q_{VP}$  into the energy equation:

$$\frac{\partial T}{\partial t} + \mathbf{u} \cdot \nabla T = \kappa \nabla^2 T + Q_{VP}, \quad (22)$$

$$Q_{VP} = \frac{\chi(\mathbf{x}, t)\rho}{\eta_t} (T_0 - T), \quad (23)$$

**Fig. 5.** Error in temperature versus for  $\delta x = 1/200, 1/240, \dots, 1/480$ .

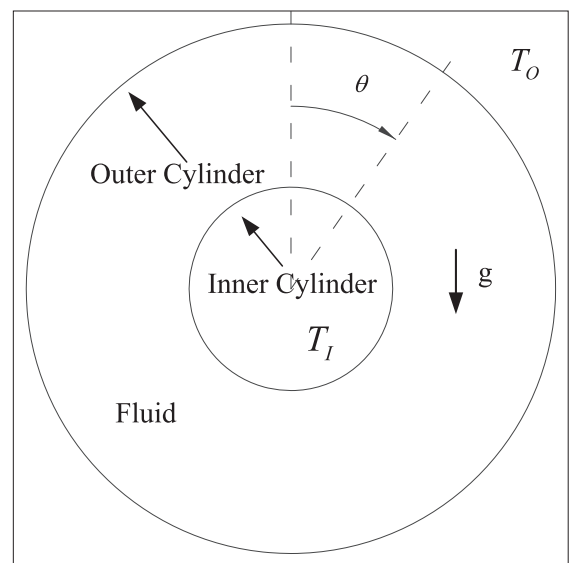
where  $\chi(\mathbf{x}, t)$  is the mask function just same as in the above LBM for flows;  $T_0$  is the temperature of the boundary and  $\eta_t \ll 1$  is the thermal penalization parameter. Here, the parameter  $\eta$  and  $\eta_t$  are set as a very small value, for instance,  $\eta = \eta_t = 10^{-8}$ .

Another population of Lattice Boltzmann equations, which are known as Thermal Lattice Boltzmann equations, is used to solve the energy equation:

$$g_z(x + e_z \Delta t, t + \Delta t) - g_z(x, t) = -\frac{g_z - g_z^{eq}}{\tau} + G_z \Delta t, \quad (24)$$

where  $g_z$  is the thermal particle distribution function;  $\tau$  is the thermal relaxation parameter;  $G_z$  is the heat source term;  $g_z^{eq}$  is the thermal equilibrium distribution function:

$$g_z^{eq} = T \omega_z \left[ 1 + \frac{\mathbf{e}_z \cdot \mathbf{u}}{c_s^2} + \frac{(\mathbf{e}_z \cdot \mathbf{u})^2 - c_s^2 \mathbf{u}^2}{2c_s^4} \right]. \quad (25)$$

**Fig. 6.** The computational domain of the natural convection between two concentrically placed horizontal circular cylinders.

For the Thermal Lattice Boltzmann method, the D2Q9 model is adopted. So the discrete velocity vectors, sonic speed and the weight factors are equal to those in the above Lattice Boltzmann method. The thermal relaxation parameter  $\tau$  is related to the thermal diffusivity  $\kappa$  through:

$$\kappa = c_s^2(\tau - 0.5)\Delta t. \quad (26)$$

The heat source is defined as [21]:

$$G_x = \left(1 - \frac{1}{2\tau}\right)\omega_x \rho Q_{vp}. \quad (27)$$

The Thermal Lattice Boltzmann equations Eq. (27) can be also solved through collision and streaming sub-steps:

$$\hat{g}_x = g_x - \frac{g_x - g_x^{eq}}{\tau} \quad (28)$$

$$g_x(\mathbf{x}, t + \Delta t) = \hat{g}_x(\mathbf{x} - \Delta \mathbf{x}_x, t). \quad (29)$$

The Macroscopic temperature is obtained by:

$$\rho T = \sum_a g_x + \frac{1}{2} Q_{vp} \Delta t. \quad (30)$$

The temperature is also divided into two parts. The first part, represented by the intermediate temperature  $T^*$ , is contributed from the thermal particles functions and the second part is contributed from the external heat source taken as temperature correction  $\delta T$ . As a result, Eq. (30) can be rewritten as:

$$T = T^* + \delta T, \quad (31)$$

in which [21]

$$T^* = \frac{1}{\rho} \sum_a g_x \quad (32)$$

$$\delta T = \frac{1}{2\rho} Q_{vp} \Delta t. \quad (33)$$

Substituting Eq. (31) into Eq. (23), the thermal penalization heat source term can be obtained as:

$$Q_{vp} = \frac{2\chi\rho(T_0 - T^*)}{2\eta_t + \chi\Delta t}, \quad (34)$$

and the temperature correction can be calculated by:

$$\delta T = \frac{\chi\Delta t(T_0 - T^*)}{2\eta_t + \chi\Delta t}. \quad (35)$$

In Summary, the general steps of the proposed algorithm are as follows.

- (1) Design the computational grid, and arrange initial values on the computational grid.
- (2) Use Eqs. (8) and (28) to obtain the density distribution functions after the collision sub-steps of the  $t = t_n$  step (initially setting  $F_x = 0$ ).
- (3) Performing the streaming sub-steps using Eqs. (9) and (29)
- (4) Use Eqs. (12), (16) and (32) to obtain the macroscopic density, the intermediate velocity and the intermediate temperature.
- (5) Use Eqs. (20) and (19) to obtain the velocity corrections and the force density.
- (6) Use Eqs. (35) and (34) to obtain the temperature corrections and the heat source term.
- (7) Correct the fluid velocity by using Eq. (18) and compute the equilibrium distribution function using Eq. (11).
- (8) Correct the temperature by using Eq. (31) and compute the thermal equilibrium distribution function using Eq. (25).

- (9) Repeat step (2) to step (8) until the convergence is reached.

In Fig. 2, all the computational steps are highlighted in the flowchart.

### 3. Numerical results and discussions

In this article, some numerical experiments are conducted to verify the present VP-TLBM method. Firstly, the heat transfer between two concentric circular cylinders, which has an analytical solution, with different grid sizes is conducted to validate the accuracy of the present method. Then the natural convection between two concentrically placed horizontal circular cylinders at different Rayleigh number and the natural convection between a cold square outer and a hot circular cylinder with different aspect ratios of the cylinder diameter to the length of the square are carried out. Finally, forced convection: flows past a heated circular cylinder and mixed convection: a heated rotating cylinder in a square enclosure experiments are carried out to validate the present method further.

#### 3.1. The heat transfer between two concentric circular cylinders

For this case, the length of the square computational domain  $L$  is set as 1 as shown in Fig. 3. The radii of the inner cylinder  $R_I$  and the outer cylinder  $R_O$  are set as 45/200 and 70/200 respectively. The centers of the inner and outer cylinders are located at the center of the computational domain. The temperatures of the inner and outer cylinders are set as 1.0 and 0.0 respectively and maintained these temperatures during the whole computational period. The relaxation parameter  $\lambda$  is equal to 0.644 and the thermal relaxation parameter  $\tau$  is 0.705. The analytical solution of this problem is

$$T(r) = \frac{T_O \log(r/R_I) - T_I \log(r/R_O)}{\log(R_O/R_I)}, \quad (36)$$

in which  $r$  is the radial coordinate.

This is a one-way interaction problem. The temperature field does not influence the flow field. So the velocity is equal to 0 everywhere during all the simulating period. The temperature field is given and analyzed only. In Fig. 4, the temperature contour and the temperature profile along the horizontal plane through the center of the cylinders are given. From the temperature profile, a good agreement can be obtained between the numerical result and the analytical solution.

To verify the accuracy of the present method for thermal flows, the same problem is simulated on nine different grid sizes:  $200 \times 200, 240 \times 240, \dots, 480 \times 480$ . The profiles of the  $L^2$  and  $L^\infty$ -errors for decreasing  $\delta x$  are shown in Fig. 5. Obviously, the error decays between  $\delta x^1$  and  $\delta x^{3/4}$ .

#### 3.2. The natural convection between two concentrically placed horizontal circular cylinders

The natural convection between two concentrically placed horizontal circular cylinders has been studied by many researchers. Here, the proposed VP-TLBM is used to study this problem to verify its capability to solve the some more complex problems. The radii of the inner and outer cylinder ratio equals to 5/13, as shown in Fig. 6. The temperature of the inner and outer cylinder is set as 1 and 0, respectively. The two cylinders are stationary. The Boussinesq approximation is used to get the buoyancy:

$$\mathbf{g} = \beta G(T - T_m) \mathbf{j}, \quad (37)$$

in which  $\beta$  is the thermal expansion parameter,  $G$  is the acceleration due to gravity,  $T_m$  is the mean temperature and  $\mathbf{j}$  represents the

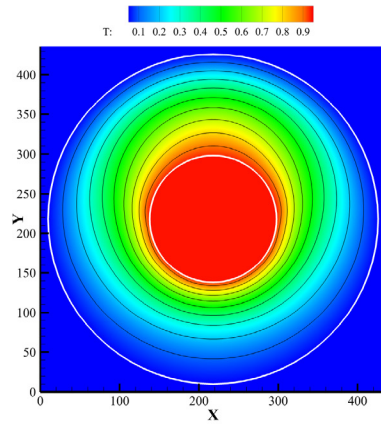
**Table 1**

Surface-averaged Nusselt numbers of the inner cylinder at  $Ra = 5 \times 10^4$  with different grids.

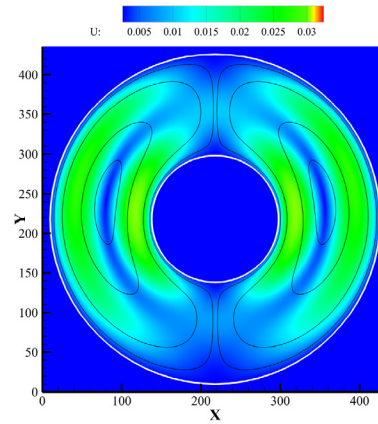
The inner cylinder radii	60	70	80	90	100
$\bar{N}_u$	3.0245	3.0253	3.0259	3.0260	3.0262

gravity direction. The non-dimensional characteristic velocity  $U_\infty$ , which is set as 0.1 here, is related to the gravity. The Prandtl number  $Pr = v/\kappa$  is equal to 0.7. The Rayleigh number is defined as:

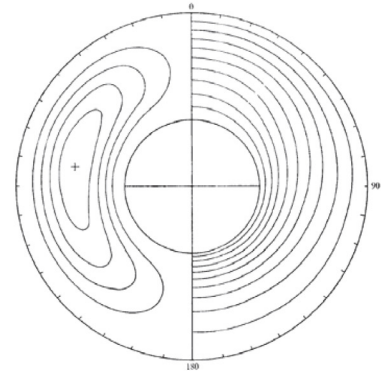
$$Ra = \beta G \Delta T L^3 / (v \kappa), \quad (38)$$



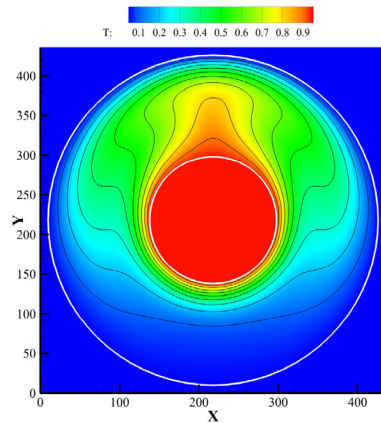
(a) Temperature contour and isotherms at  $Ra = 10^3$



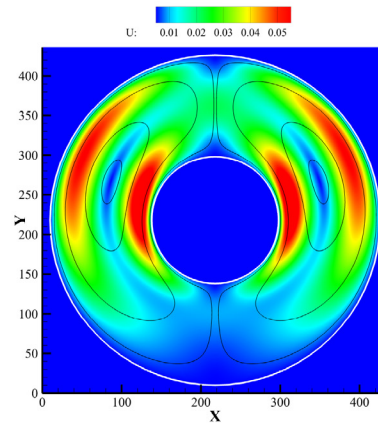
(b) Streamlines and velocity contour at  $Ra = 10^3$



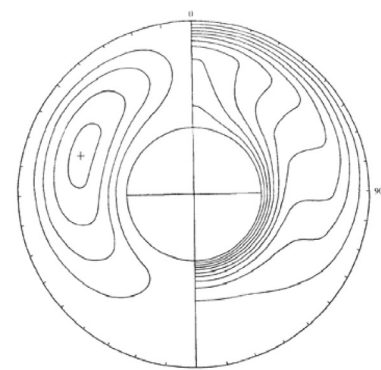
(c) The result and figure of the previous experiment [27]



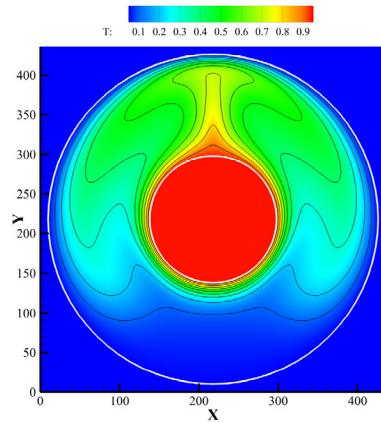
(d) Temperature contour and isotherms at  $Ra = 10^4$



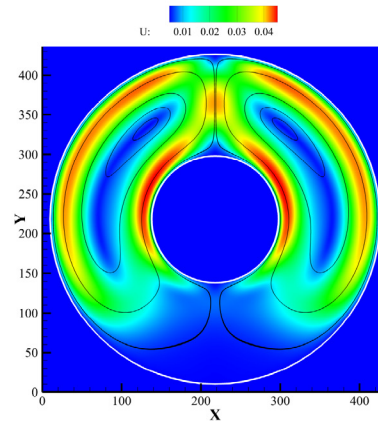
(e) Streamlines and velocity contour at  $Ra = 10^4$



(f) The result and figure of the previous experiment [27]



(g) Temperature contour and isotherms at  $Ra = 5 \times 10^4$



(h) Streamlines and velocity contour at  $Ra = 5 \times 10^4$



(i) The result and figure of the previous experiment [27]

**Fig. 7.** Temperature contours, isotherms, streamlines and velocity contours for the natural convection between two concentric circular cylinders with  $Pr = 0.7$  and  $U_\infty = 0.1$  at different Rayleigh numbers  $Ra = 10^3, 10^4$  and  $5 \times 10^4$ . The results and figures of the previous literature [27] are given.

where  $\Delta T$  is the temperature difference, which is equal to  $T_I - T_O$ .  $L$  is the characteristic length which is defined as  $L = R_O - R_I$ . The surface-averaged Nusselt number, which is defined as

$$\bar{N}_u = \frac{1}{W} \int_0^W \left( -\frac{\partial T}{\partial n} \right)_{\text{wall}} ds, \quad (39)$$

in which  $n$  is the outward unit vector normal to the cylinder surface, whose circumferential length is  $W$ . In this article, three different numerical experiments with the same Prandtl number  $Pr = 0.7$  and non-dimensional characteristic velocity  $U_\infty = 0.1$  at different Rayleigh numbers  $Ra = 10^3, 10^4$  and  $5 \times 10^4$  are conducted.

Firstly, grid dependence test is conducted with  $Ra = 5 \times 10^4$ . Five different grids in which the radii of the inner cylinder is 60, 70, 80, 90 and 100 are tested. From the results in Table 1, the grid in which the radii of the inner cylinder is 80 can be chosen as the computation grid.

In Fig. 7, the temperature contours, isotherms, streamlines and velocity contours are shown. The centers of the two vortices go upper and the isotherms on the upper part become more distorted when the Rayleigh number grows, which means convection dominates the flow and temperature fields with Rayleigh number increasing [22]. These results agree well with the previous reports in [27].

The non-dimensional temperature and angular velocity profiles are compared with the result obtain by Seta [21] at  $Ra = 5 \times 10^4$  are give in Fig. 8. Good agreement has been obtained between the present results and the previous results.

### 3.3. The natural convection between a cold square outer and a hot circular cylinder

The convection between a cold square outer, the temperature of which is 0, and a hot circular cylinder inner, the temperature of which is equal to 1, numerical experiments are conducted to verify the capability of the present method further. The computational domain is shown in Fig. 9. The length of the outer square is  $L$ . The Prandtl number  $Pr$  is set as 0.71 and the non-dimensional velocity  $U_\infty$  is equal to 0.07 for all experiments. Three Rayleigh number  $Ra = 10^4, 10^5$  and  $10^6$  are adopted. For each Rayleigh number, cylinders with three different radii  $R_I = 0.1L, 0.2L$  and  $0.3L$  are performed. Firstly, grid dependence test is conducted with  $Ra = 10^6$  and  $R_I = 0.1L$ . Four different grids in which the length of the outer square is 300, 400, 500 and 600 are tested. From the

results in Table 2, the grid in which the radii of the inner cylinder is 500 can be chosen as the computation grid.

Figs. 10–12 show the temperature and velocity contours of the experiments, as well as the streamlines and isotherms. The streamlines and isotherms agree well with the results given in [21]. We also study the surface-averaged Nusselt number. A second order approximation is adopted to get the temperature gradient  $\frac{\partial T}{\partial n}$ . The comparison is given in Table 3, from which good agreement can be obtained between the present results and the data in previous literatures.

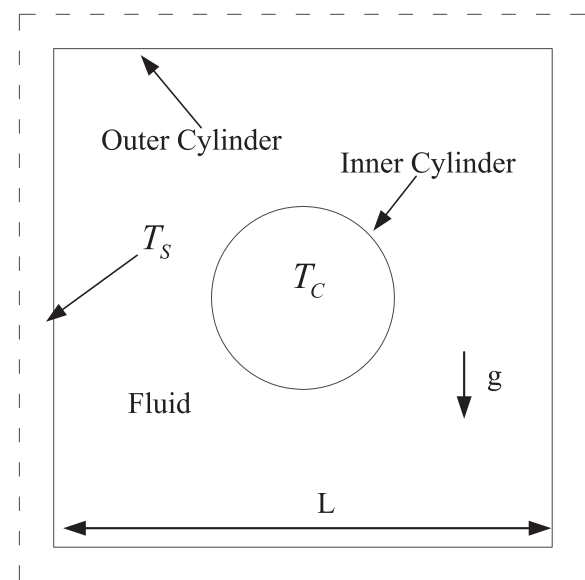


**Fig. 9.** The computational domain of the natural convection between a cold square outer and a hot circular cylinder.

**Table 2**  
Surface-averaged Nusselt numbers of the inner cylinder at  $Ra = 10^6$  with different grids.

Length of the outer square	300	400	500	600
$\bar{N}_u$	6.4245	6.4249	6.4252	6.4254

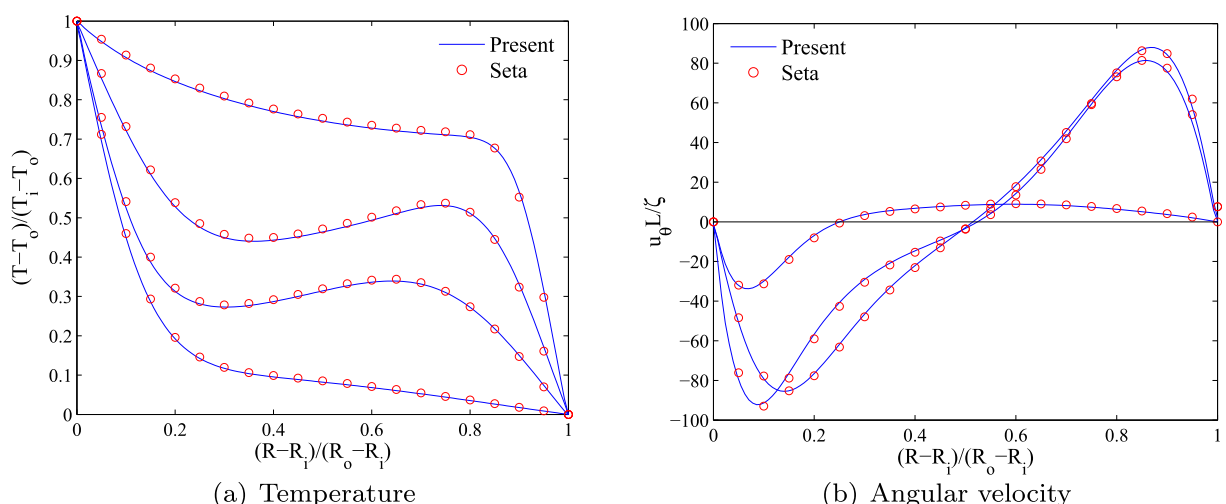


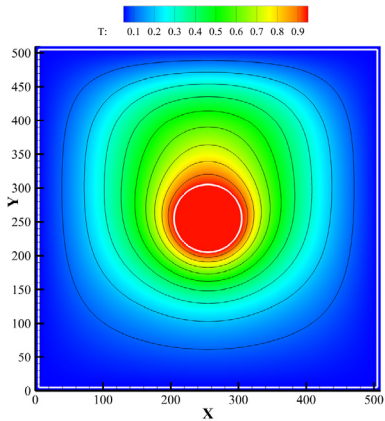
**Fig. 8.** Non-dimensional temperature and angular velocity between the two cylinders.

### 3.4. Flows past a heated circular cylinder

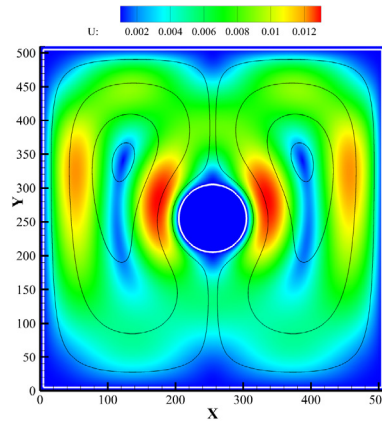
As a typical forced convection experiment, the flow past a heated circular cylinder has been studied by many researchers,

such as Hu et al. [29] and Ren et al. [30]. The Reynolds number ( $Re$ ) is defined as

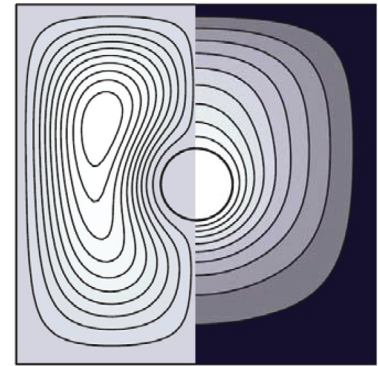
$$Re = \frac{U_{\max}D}{\mu}, \quad (40)$$



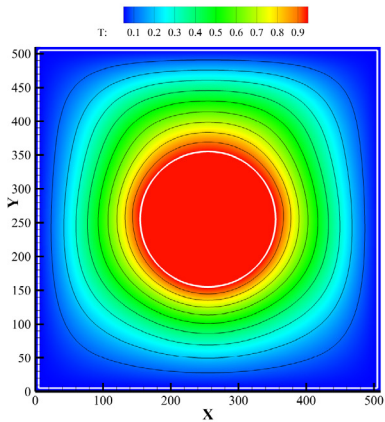
(a) Temperature contour and isotherms with  $R_I = 0.1L$



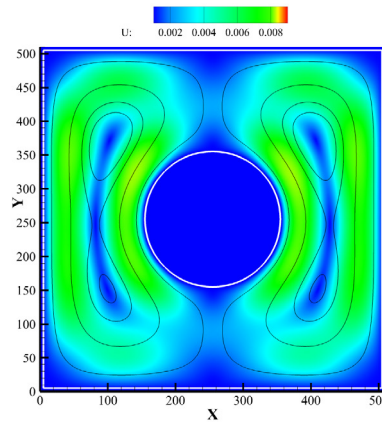
(b) Streamlines and velocity contour with  $R_I = 0.1L$



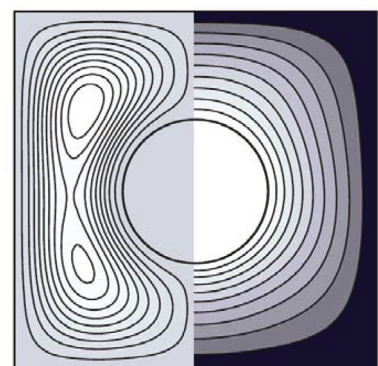
(c) The result and figure given by Seta[21]



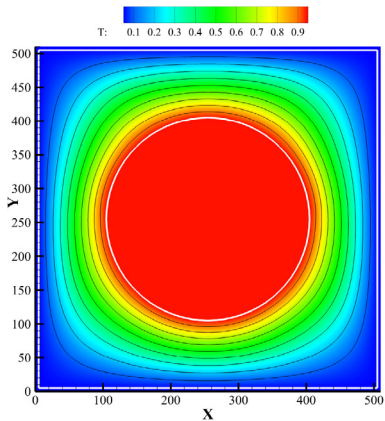
(d) Temperature contour and isotherms with  $R_I = 0.2L$



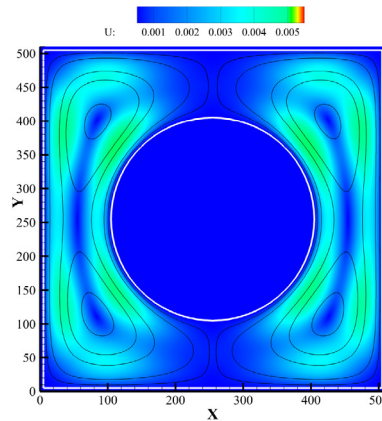
(e) Streamlines and velocity contour with  $R_I = 0.2L$



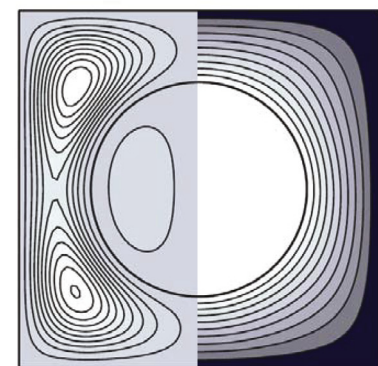
(f) The result and figure given by Seta[21]



(g) Temperature contour and isotherms with  $R_I = 0.3L$



(h) Streamlines and velocity contour with  $R_I = 0.3L$



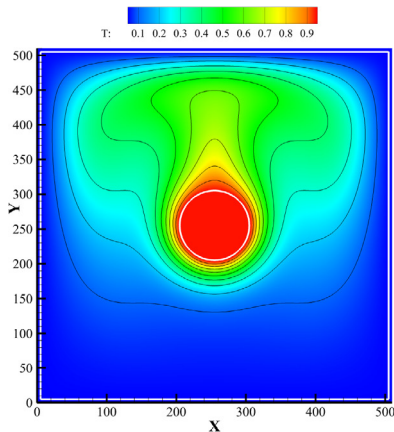
(i) The result and figure given by Seta[21]

**Fig. 10.** Temperature contours, isotherms, streamlines and velocity contours for the natural convection between a square outer and a cylinder inner at Rayleigh numbers  $Ra = 10^4$ . The results and figures given by Seta [21] are also given.

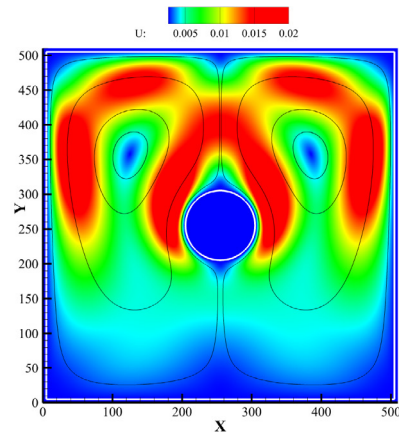
where  $U_{\max}$  is the free stream velocity and  $D$  is the diameter of the heated cylinder. The drag coefficient of the cylinder is defined as

$$C_d = \frac{2F_D}{\rho U_{\max}^2 D}, \quad (41)$$

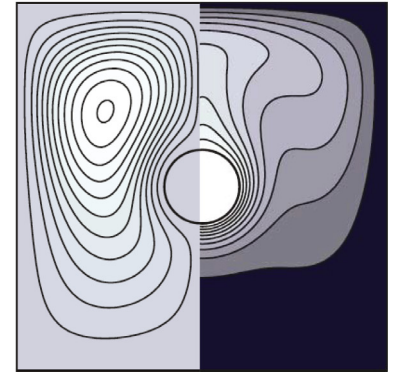
where  $F_D$  is the drag force. The computational domain is a rectangular domain with a size of  $30D \times 20D$ , which is adopted by Hu et al. [29], as shown in Fig. 13. The heated cylinder is located at  $(8D, 10D)$ . The free stream velocity is set as 0.1, and the Prandtl number



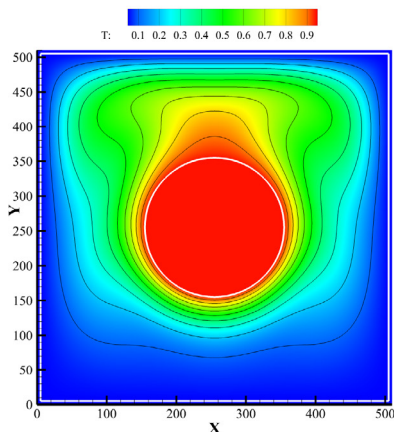
(a) Temperature contour and isotherms with  $R_I = 0.1L$



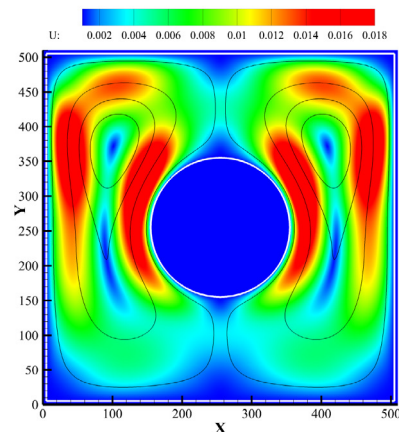
(b) Streamlines and velocity contour with  $R_I = 0.1L$



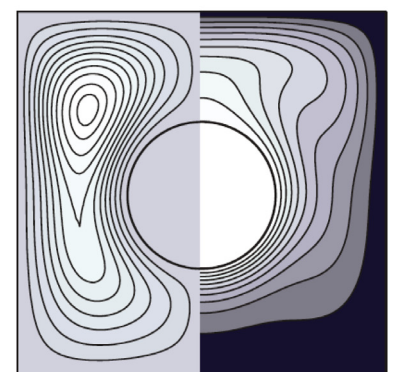
(c) The result and figure given by Seta[21]



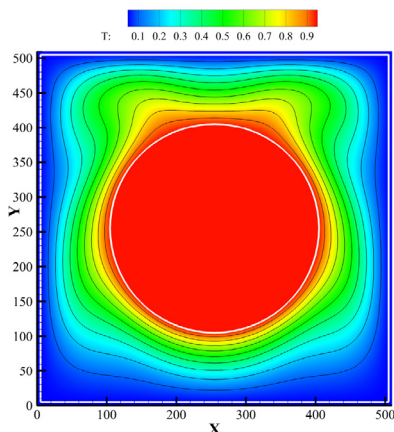
(d) Temperature contour and isotherms with  $R_I = 0.2L$



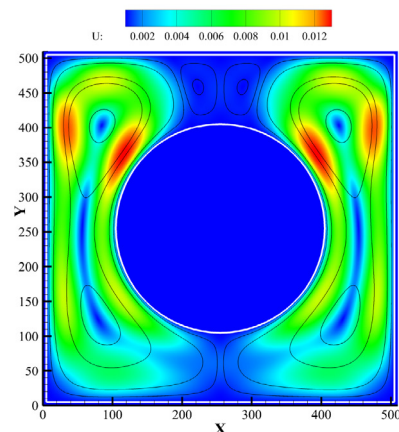
(e) Streamlines and velocity contour with  $R_I = 0.2L$



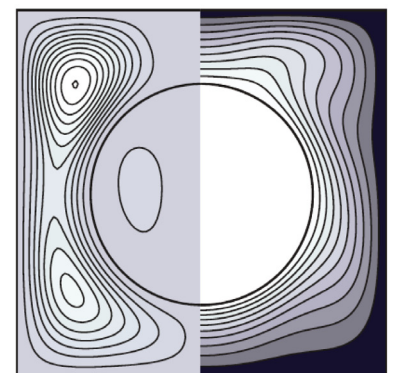
(f) The result and figure given by Seta[21]



(g) Temperature contour and isotherms with  $R_I = 0.3L$

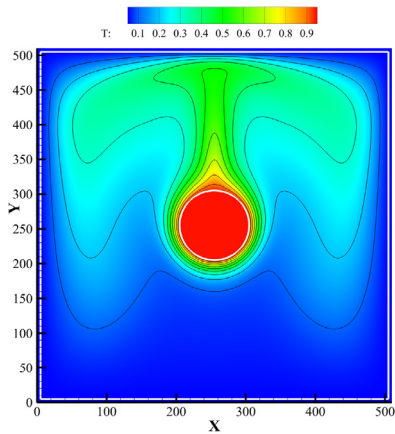


(h) Streamlines and velocity contour with  $R_I = 0.3L$

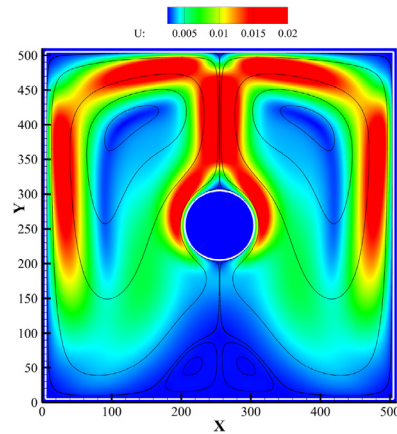


(i) The result and figure given by Seta[21]

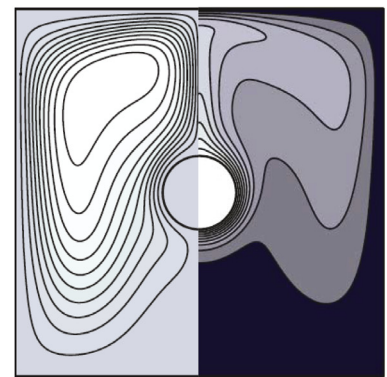
**Fig. 11.** Temperature contours, isotherms, streamlines and velocity contours for the natural convection between a square outer and a cylinder inner at Rayleigh numbers  $Ra = 10^5$ . The results and figures given by Seta [21] are also given.



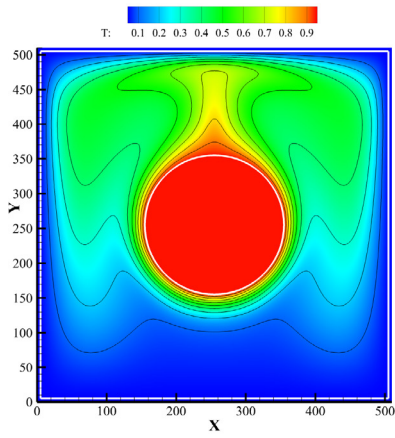
(a) Temperature contour and isotherms with  $R_I = 0.1L$



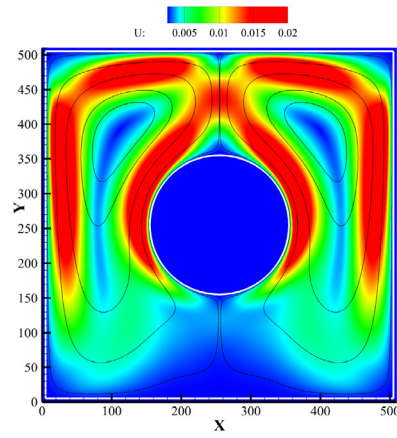
(b) Streamlines and velocity contour with  $R_I = 0.1L$



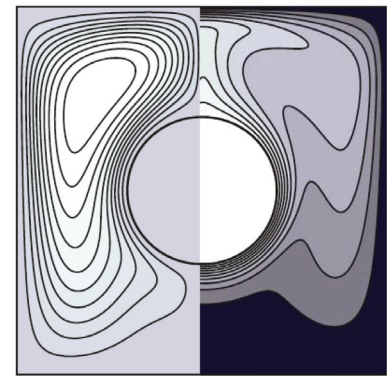
(c) The result and figure given by Seta[21]



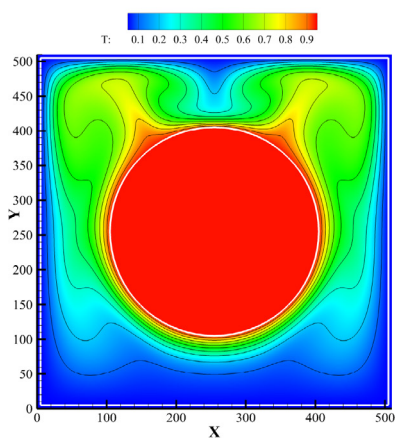
(d) Temperature contour and isotherms with  $R_I = 0.2L$



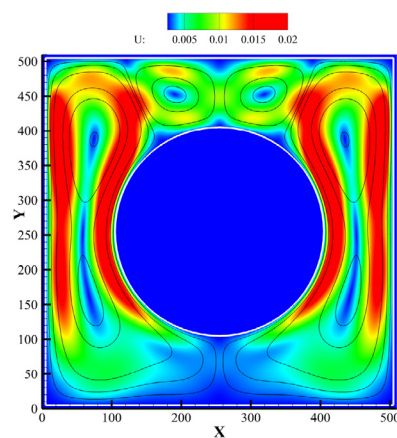
(e) Streamlines and velocity contour with  $R_I = 0.2L$



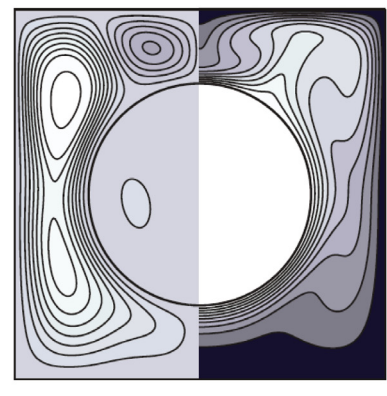
(f) The result and figure given by Seta[21]



(g) Temperature contour and isotherms with  $R_I = 0.3L$



(h) Streamlines and velocity contour with  $R_I = 0.3L$



(i) The result and figure given by Seta[21]

**Fig. 12.** Temperature contours, isotherms, streamlines and velocity contours for the natural convection between a square outer and a cylinder inner at Rayleigh numbers  $Ra = 10^6$ . The results and figures given by Seta [21] are also given.

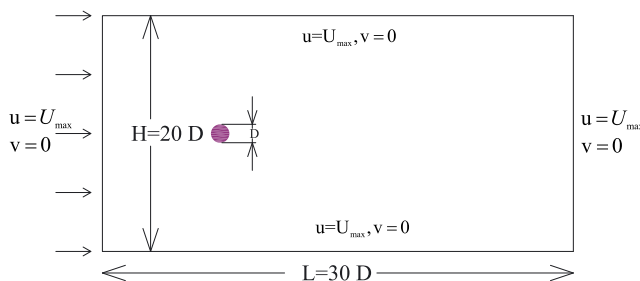
$Pr = 0.7$ . In the inlet, top, bottom and outlet boundaries, the temperature is set to 0.0, and the temperature of the circular cylinder is set as 1.0.

Different grids  $600 \times 400, 900 \times 600, 1200 \times 800$  and  $1500 \times 1000$  are used in the flows past a heated cylinder at  $Re = 20$  experiment to study the effect of grid refinement on

**Table 3**

Comparison of the surface averaged Nusselt number.

$Ra$	$R_l$	Sete [21]	Shu et al. [28]	Present
$10^4$	$0.1L$	2.206	2.08	2.160
	$0.2L$	3.461	3.24	3.361
	$0.3L$	5.832	5.40	5.621
$10^5$	$0.1L$	3.987	3.79	3.891
	$0.2L$	5.253	4.86	5.199
	$0.3L$	6.685	6.21	6.581
$10^6$	$0.1L$	6.542	6.11	6.425
	$0.2L$	9.547	8.90	9.378
	$0.3L$	12.87	12.0	12.911

**Fig. 13.** The computational domain of flows past a heated circular cylinder.**Table 4**Surface-averaged Nusselt numbers for flows past a heated cylinder at  $Re = 20$  with different grids.

Grid	$600 \times 400$	$900 \times 600$	$1200 \times 800$	$1500 \times 1000$
$\bar{N}_u$	2.472	2.455	2.451	2.449

surface-averaged Nusselt number. From **Table 4**, the results of grid ( $1200 \times 800$ ) and grid ( $1500 \times 1000$ ) are closer to each other. In our experiments, the grid ( $1200 \times 800$ ) is adopted.

The flows past a heated circular cylinder is a one-way interaction problem. The temperature does not influence the flow field, which means the flows past a heated circular cylinder is the same as the flows past a non-heated cylinder. The drag coefficient  $C_d$ , the recirculation region  $L_s$  and the separation angle  $\theta_s$  are compared with the results of flows past a non-heated cylinder in the previous literatures in **Table 5**. The comparison of the surface average Nusselt number is given in **Table 6**. In **Fig. 14**, the streamlines and isotherms of our experiments and the experiments conducted by Hu et al. [29] are given. It can be seen the present results agree well with the results given in the previous literatures, which means our method can be used to solve the forced convection problems.

### 3.5. Mixed convection of a heated rotating cylinder in a square enclosure

Mixed convection is a combination of forced convection and natural convection. To validate our method further, mixed convection of a heated rotating cylinder in a square enclosure is conducted.

The schematic configuration of a heated rotating cylinder in a square enclosure is given in **Fig. 15**. The length of the outer square is  $L$ , and the diameter of the inner circular cylinder is  $D$ . The temperatures of the inner cylinder and the outer square are set as 1.0 and 0.0. The inner cylinder rotates at a angular velocity  $\omega$ , which

**Table 5**Drag coefficient, length of bubbles and separation angle for flows past a heated cylinder at  $Re = 20$  and  $Re = 40$ .

Case	References	$C_d$	$L_s$	$\theta_s$
$Re = 20$	Cui et al. [31]	2.11	0.93	42.8°
	Guo et al. [14]	2.11	0.919	42.9°
	Hu et all. [29]	2.153	0.88	–
	Present	2.13	0.935	42.8°
$Re = 40$	Cui et al. [31]	1.56	2.20	53.0°
	Guo et al. [14]	1.58	2.24	52.8°
	Hu et all. [29]	1.618	2.24	–
	Present	1.60	2.201	52.9°

**Table 6**Surface-averaged Nusselt numbers for flows past a heated cylinder at  $Re = 20$  and  $Re = 40$ .

	$Re = 20$	$Re = 40$
Present	2.45	3.29
Hu et al. [29]	2.43	3.26
Ren et al. [30]	2.52	3.35
Haeri et al. [32]	2.38	3.15

means the maximum velocity of the rotating cylinder is  $U_{max} = \omega D/2$ . Another important parameter in the mixed convection is Richardson number ( $Ri$ ), which is used to evaluate the relative importance of the natural and forced convection. The Richardson number is defined as  $Ri = \frac{Ra}{PrRe^2}$ . In our experiments, the maximum velocity of the rotating cylinder is set as 0.1, the Prandtl number  $Pr = 0.71$  and the Richardson number is set as 10.0. The square enclosure length and cylinder diameter ratio ( $L/D$ ) equals to 2.5. Three experiments with  $Ra = 10^4$ ,  $Ra = 10^5$  and  $Ra = 10^6$  are conducted.

Firstly, grid dependence test is conducted with  $Ra = 10^6$ . Four different grids  $300 \times 300$ ,  $400 \times 400$ ,  $500 \times 500$  and  $600 \times 600$  are tested. From the results in **Table 7**, a grid size of  $500 \times 500$  can be chosen as the computation grid. The averaged Nusselt numbers for the mixed convection of a heated rotating cylinder in a square enclosure at  $Ra = 10^4$ ,  $Ra = 10^5$  and  $Ra = 10^6$  are given in **Table 8**, and the isotherms and streamlines are given in **Fig. 16**. Also the results of Liao and Lin [33] are shown. It can be seen that our presents agree well with the results in the previous literature, which means our method can be used to simulated the mixed convection problems.

## 4. Conclusions

In this article, a coupled Volume Penalization-Thermal Lattice Boltzmann method is proposed to simulate the incompressible viscous thermal flows. The double distribution Lattice Boltzmann model is used to solve the thermal flow equations. An external force term based on the Volume Penalization method is introduced into the athermal Lattice Boltzmann equations to reflect the effect of the boundaries on the flows. An external thermal penalization heat source term is proposed and added into the thermal Lattice Boltzmann equations to reflect the Dirichlet thermal boundary conditions. To perform the proposed Volume Penalization-Thermal Lattice Boltzmann method on a certain Lagrangian point, only the variables of one certain Euler point coinciding the Lagrangian point are needed, which means the whole procedure can be conducted parallelly. To validate the accuracy of the proposed method, the heat transfer between two concentric circular

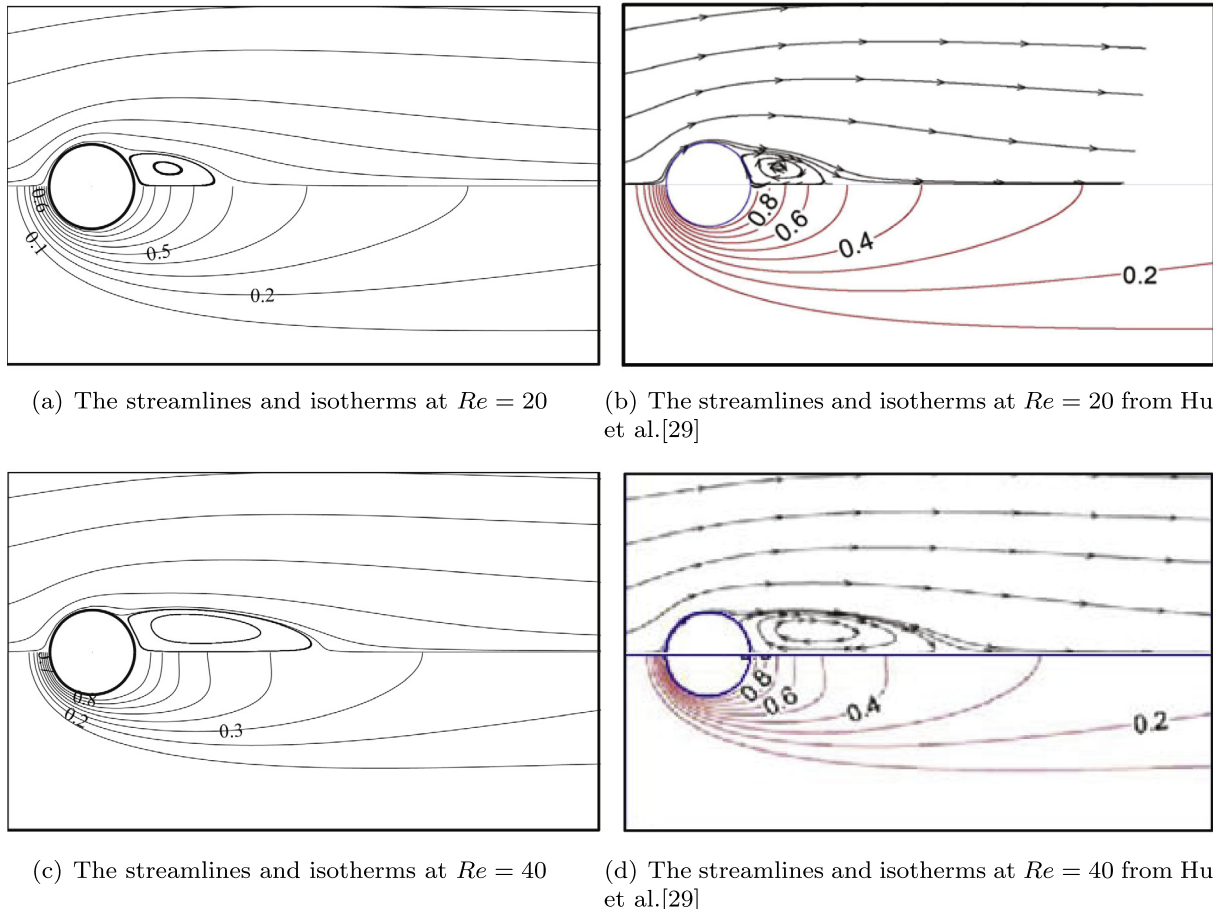


**Fig. 14.** Streamlines and isotherms for the flows past a heated circular cylinder at  $Re = 20$  and  $Re = 40$ . The results and figures of the previous literature [29] are also given.

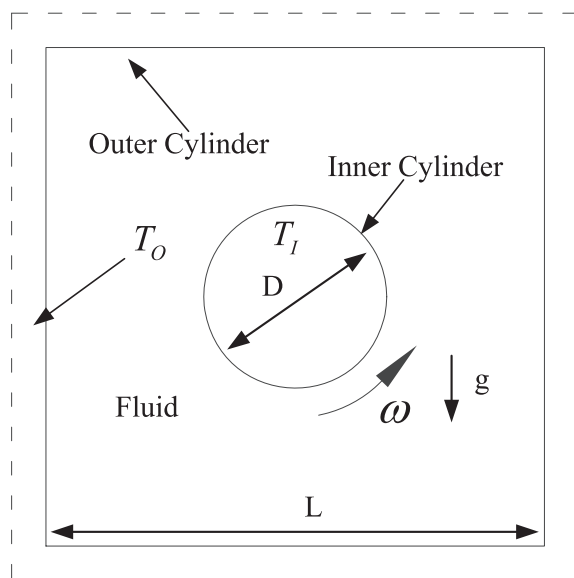


**Fig. 15.** The computational domain of a heated rotating cylinder in a square enclosure.

cylinders experiments are conducted on different grid sizes. The natural convection between two concentric circular cylinders and the natural convection between a cold square outer and a hot

**Table 7**

Surface-averaged Nusselt numbers for the mixed convection of a heated rotating cylinder in a square enclosure at  $Ra = 10^6$  with different grids.

Grid	$300 \times 300$	$400 \times 400$	$500 \times 500$	$600 \times 600$
$\bar{N}_u$	15.098	15.178	15.182	15.184

**Table 8**

Surface-averaged Nusselt numbers for the mixed convection of a heated rotating cylinder in a square enclosure.

$\bar{N}_u$	$Ra = 10^4$	$Ra = 10^5$	$Ra = 10^6$
Present	6.409	9.012	15.182
Liao and Lin [33]	6.41	9.00	15.20

circular cylinder inner are performed to verify the present method further. To validate the ability of the method to solve the forced convection and mixed convection, the flows past a heated circular cylinder and the mixed convection of a heated rotating cylinder in a square enclosure are conducted.

From the comparison between the present numerical results and the data in the previous literatures, good agreements are obtained. Although the current method is developed and validated in 2D, it is easy to extend the present method to 3D by replacing thermal D2Q9 lattice model with thermal D3Q15 or D3Q19 lattice model.

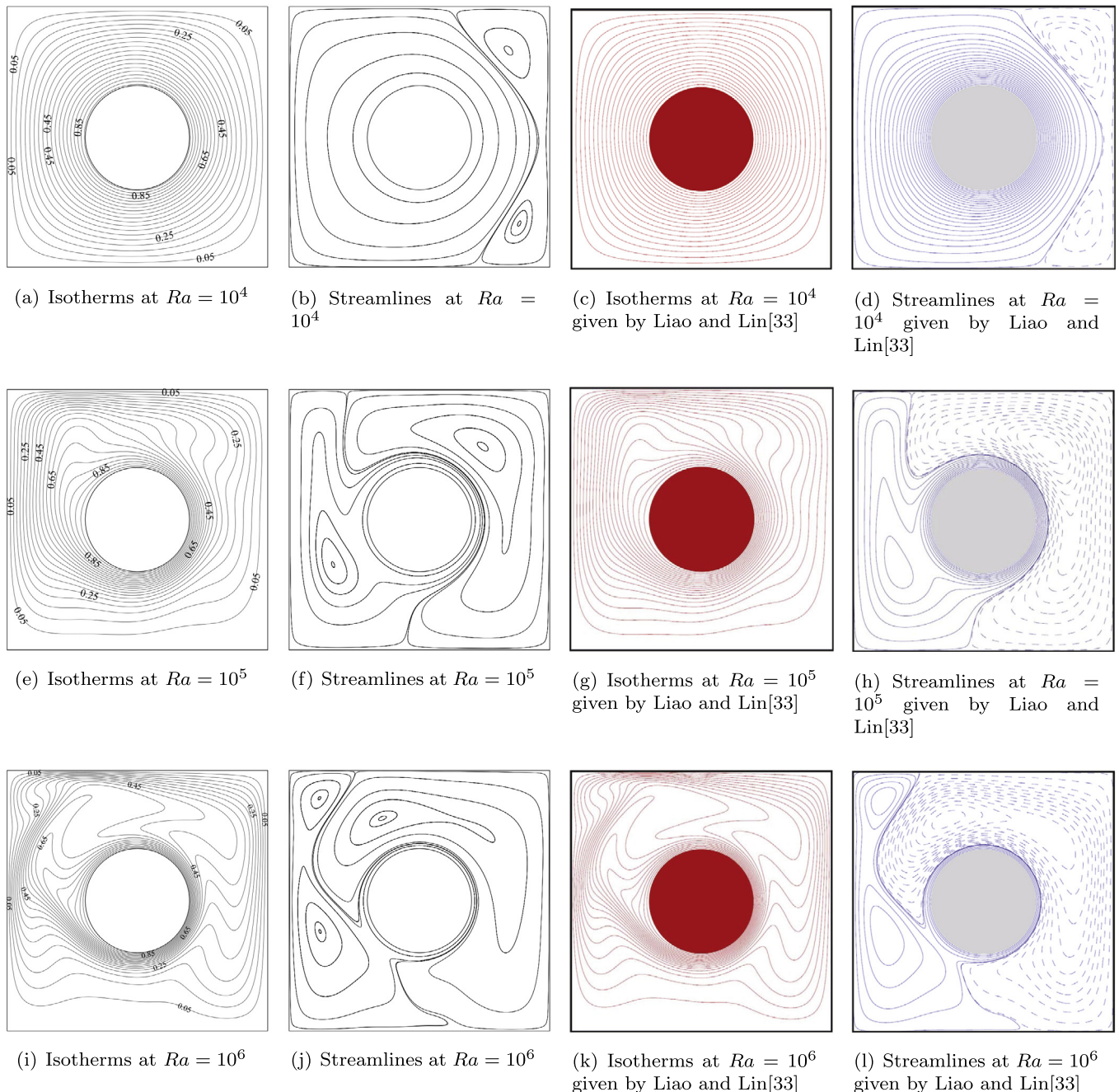


**Fig. 16.** Isotherms and streamlines for the mixed convection of a heated rotating cylinder in a square enclosure with  $Pr = 0.71$  at different Rayleigh numbers  $Ra = 10^4, 10^5$  and  $10^6$ . The results and figures of the previous literature [33] are also given.

## Conflict of interest

Authors declare that there is no conflict of interest.

## Acknowledgements

The authors would like to thank Prof. Seta for his greatly useful help and advice about the Thermal Lattice Boltzmann. The authors would also like to acknowledge the support of the Fundamental Research Funds for the Central Universities (HEUCFP201744) and the National Nature Science Foundation of China (51779056).

## References

- [1] S. Chen, G.D. Doolen, Lattice Boltzmann method for fluid flows, *Annu. Rev. Fluid Mech.* 30 (1) (1998) 329–364, <https://doi.org/10.1146/annurev.fluid.30.1.329>.
- [2] A. Piquet, O. Roussel, A. Hadjadj, A comparative study of Brinkman penalization and direct-forcing immersed boundary methods for compressible viscous flows, *Comput. Fluids* 136 (Supplement C) (2016) 272–284, <https://doi.org/10.1016/j.compfluid.2016.06.001>. <<http://www.sciencedirect.com/science/article/pii/S0045793016301882>>.
- [3] C.S. Peskin, The immersed boundary method, *Acta Numer.* 11 (2002) 479–517, <https://doi.org/10.1017/S0962492902000077>.
- [4] Z.-G. Feng, E.E. Michaelides, The immersed boundary-lattice Boltzmann method for solving fluid-particles interaction problems, *J. Comput. Phys.* 195 (2) (2004) 602–628, <https://doi.org/10.1016/j.jcp.2003.10.013>. <<http://www.sciencedirect.com/science/article/pii/S0021999103005758>>.

- [5] M. Uhlmann, An immersed boundary method with direct forcing for the simulation of particulate flows, *J. Comput. Phys.* 209 (2) (2005) 448–476, <https://doi.org/10.1016/j.jcp.2005.03.017>. <<http://www.sciencedirect.com/science/article/pii/S0021999105001385>>.
- [6] J. Wu, C. Shu, Implicit velocity correction-based immersed boundary-lattice Boltzmann method and its applications, *J. Comput. Phys.* 228 (6) (2009) 1963–1979, <https://doi.org/10.1016/j.jcp.2008.11.019>. <<http://www.sciencedirect.com/science/article/pii/S0021999108006116>>.
- [7] X. Niu, C. Shu, Y. Chew, Y. Peng, A momentum exchange-based immersed boundary-lattice Boltzmann method for simulating incompressible viscous flows, *Phys. Lett. A* 354 (3) (2006) 173–182, <https://doi.org/10.1016/j.physleta.2006.01.060>. <<http://www.sciencedirect.com/science/article/pii/S0375960106001472>>.
- [8] E. Arquis, J. Caltagirone, Sur les conditions hydrodynamiques au voisinage d'une interface milieu fluide-milieu poreux: application la convection naturelle, *C.R. Acad. Sci. Paris* 299 (1) (1984) 1–4, cited By 106.
- [9] M. Benamour, E. Liberge, C. Bghein, Lattice Boltzmann method for fluid flow around bodies using volume penalization, *Int. J. Multiphys.* 9 (3) (2016), <https://doi.org/10.1260/1750-9548.9.3.299>. <<http://journal.multiphysics.org/index.php/IJM/article/view/294>>.
- [10] P. Angot, C.-H. Bruneau, P. Fabrie, A penalization method to take into account obstacles in incompressible viscous flows, *Numer. Math.* 81 (4) (1999) 497–520, <https://doi.org/10.1007/s002110050401>.
- [11] Gilles Carbot, Pierre Fabrie, Boundary layer for a penalization method for viscous incompressible flow, *Adv. Differ. Eq.* 8 (12) (2003) 1453–1480.
- [12] T. Engels, D. Kolomenskiy, K. Schneider, J. Sesterhenn, Numerical simulation of fluid–structure interaction with the volume penalization method, *J. Comput. Phys.* 281 (2015) 96–115, <https://doi.org/10.1016/j.jcp.2014.10.005>. <<http://www.sciencedirect.com/science/article/pii/S0021999114006792>>.
- [13] Z. Guo, C. Zheng, B. Shi, Discrete lattice effects on the forcing term in the lattice Boltzmann method, *Phys. Rev. E* 65 (2002) 046308, <https://doi.org/10.1103/PhysRevE.65.046308>. <<http://link.aps.org/doi/10.1103/PhysRevE.65.046308>>.
- [14] K. Guo, X. Cui, M. Liu, A coupled lattice Boltzmann-volume penalization for flows past fixed solid obstacles with local mesh refinement, *Math. Problems Eng.* (2018), <https://doi.org/10.1155/2018/6732082>.
- [15] J.P. Kumar, J. Umavathi, A.J. Chamkha, I. Pop, Fully-developed free-convective flow of micropolar and viscous fluids in a vertical channel, *Appl. Math. Model.* 34 (5) (2010) 1175–1186, <https://doi.org/10.1016/j.apm.2009.08.007>. <<http://www.sciencedirect.com/science/article/pii/S0307904X09002352>>.
- [16] A.J. Chamkha, Flow of two-immiscible fluids in porous and nonporous channels, *J. Fluids Eng.* 122 (1) (2010) 117–124, <https://doi.org/10.1115/1.483233>. <<http://www.sciencedirect.com/science/article/pii/S0307904X09002352>>.
- [17] M. Sheikholeslami, S. Shehzad, Simulation of water based nanofluid convective flow inside a porous enclosure via non-equilibrium model, *Int. J. Heat Mass Transf.* 120 (2018) 1200–1212, <https://doi.org/10.1016/j.ijheatmasstransfer.2017.12.132>. <<http://www.sciencedirect.com/science/article/pii/S0017931017347658>>.
- [18] M. Sheikholeslami, Numerical investigation of nanofluid free convection under the influence of electric field in a porous enclosure, *J. Mol. Liq.* 249 (2018) 1212–1221, <https://doi.org/10.1016/j.molliq.2017.11.141>. <<http://www.sciencedirect.com/science/article/pii/S0167732217346391>>.
- [19] M. Sheikholeslami, M. Seyednezhad, Simulation of nanofluid flow and natural convection in a porous media under the influence of electric field using CVFEM, *Int. J. Heat Mass Transf.* 120 (2018) 772–781, <https://doi.org/10.1016/j.ijheatmasstransfer.2017.12.087>. <<http://www.sciencedirect.com/science/article/pii/S0017931017346124>>.
- [20] M. Sheikholeslami, H.B. Rokni, Numerical simulation for impact of coulomb force on nanofluid heat transfer in a porous enclosure in presence of thermal radiation, *Int. J. Heat Mass Transf.* 118 (2018) 823–831, <https://doi.org/10.1016/j.ijheatmasstransfer.2017.11.041>. <<http://www.sciencedirect.com/science/article/pii/S001793101733987X>>.
- [21] T. Seta, Implicit temperature-correction-based immersed-boundary thermal lattice Boltzmann method for the simulation of natural convection, *Phys. Rev. E* 87 (2013) 063304, <https://doi.org/10.1103/PhysRevE.87.063304>. <<http://link.aps.org/doi/10.1103/PhysRevE.87.063304>>.
- [22] J. Wu, Y. Cheng, L.A. Miller, An iterative source correction based immersed boundary-lattice Boltzmann method for thermal flow simulations, *Int. J. Heat Mass Transf.* 115 (Part B) (2017) 450–460, <https://doi.org/10.1016/j.ijheatmasstransfer.2017.08.004>. <<http://www.sciencedirect.com/science/article/pii/S0017931017318409>>.
- [23] M.-F. Chen, X.-D. Niu, Y.-R. Ma, H. Yamaguchi, Y. Iwamoto, An improved momentum-exchanged immersed boundary-based lattice Boltzmann method for incompressible viscous thermal flows, *Procedia Eng.* 126 (2015) 691–695, <https://doi.org/10.1016/j.proeng.2015.11.271>, frontiers in Fluid Mechanics Research <<http://www.sciencedirect.com/science/article/pii/S1877705815036000>>.
- [24] M. Sheikholeslami, M. Gorji-Bandpy, K. Vajravelu, Lattice Boltzmann simulation of magnetohydrodynamic natural convection heat transfer of Al<sub>2</sub>O<sub>3</sub>-water nanofluid in a horizontal cylindrical enclosure with an inner triangular cylinder, *Int. J. Heat Mass Transf.* 80 (2015) 16–25, <https://doi.org/10.1016/j.ijheatmasstransfer.2014.08.090>. <<http://www.sciencedirect.com/science/article/pii/S0017931014007881>>.
- [25] T. Lee, C.-L. Lin, An Eulerian description of the streaming process in the lattice Boltzmann equation, *J. Comput. Phys.* 185 (2) (2003) 445–471, [https://doi.org/10.1016/S0021-9991\(02\)00065-7](https://doi.org/10.1016/S0021-9991(02)00065-7). <<http://www.sciencedirect.com/science/article/pii/S0021999102000657>>.
- [26] Z. Guo, C. Zheng, B. Shi, Discrete lattice effects on the forcing term in the lattice Boltzmann method, *Phys. Rev. E Stat. Nonlinear Soft Matter Phys.* 65 (4 Pt 2B) (2002) 110–126.
- [27] T.H. Kuehn, R.J. Goldstein, An experimental and theoretical study of natural convection in the annulus between horizontal concentric cylinders, *J. Fluid Mech.* 74 (4) (2006) 695–719.
- [28] C. Shu, Y.D. Zhu, Efficient computation of natural convection in a concentric annulus between an outer square cylinder and an inner circular cylinder, *Int. J. Numer. Meth. Fluids* 38 (5) (2002) 429–445, <https://doi.org/10.1002/fld.226>.
- [29] Y. Hu, D. Li, S. Shu, X. Niu, An efficient smoothed profile-lattice Boltzmann method for the simulation of forced and natural convection flows in complex geometries, *Int. Commun. Heat Mass Transf.* 68 (2015) 188–199, <https://doi.org/10.1016/j.icheatmasstransfer.2015.05.030>. <<http://www.sciencedirect.com/science/article/pii/S0735193315001414>>.
- [30] W. Ren, C. Shu, J. Wu, W. Yang, Boundary condition-enforced immersed boundary method for thermal flow problems with Dirichlet temperature condition and its applications, *Comput. Fluids* 57 (2012) 40–51, <https://doi.org/10.1016/j.compfluid.2011.12.006>. <<http://www.sciencedirect.com/science/article/pii/S0045793011003690>>.
- [31] X. Cui, X. Yao, Z. Wang, M. Liu, A hybrid wavelet-based adaptive immersed boundary finite-difference lattice Boltzmann method for two-dimensional fluid–structure interaction, *J. Comput. Phys.* 333 (Supplement C) (2017) 24–48, <https://doi.org/10.1016/j.jcp.2016.12.019>. <<http://www.sciencedirect.com/science/article/pii/S0021999116306726>>.
- [32] S. Haeri, J. Shrimpton, A new implicit fictitious domain method for the simulation of flow in complex geometries with heat transfer, *J. Comput. Phys.* 237 (2013) 21–45, <https://doi.org/10.1016/j.jcp.2012.11.050>. <<http://www.sciencedirect.com/science/article/pii/S0021999112007322>>.
- [33] C.-C. Liao, C.-A. Lin, Mixed convection of a heated rotating cylinder in a square enclosure, *Int. J. Heat Mass Transf.* 72 (2014) 9–22, <https://doi.org/10.1016/j.ijheatmasstransfer.2013.12.081>. <<http://www.sciencedirect.com/science/article/pii/S0017931014000143>>.